BIOCHEMISTRY
including biophysical chemistry & molecular biology

Article

pubs.acs.org/biochemistry

Preparation Protocols of Aβ(1−40) Promote the Formation of Polymorphic Aggregates and Altered Interactions with Lipid Bilayers

Elizabeth A. Yates[†,∥] and Justin Legleiter*[,†,‡,§]

[†]The C. Eugene Bennett Department of Chemistry, West Virginia University, 217 Clark Hall, Morgantown, West Virginia 26506, United States

[‡]NanoSAFE, West Virginia University, P.O. Box 6223, Morgantown, West Virginia 26506, United States

[§]Center for Neuroscience, Robert C. Byrd Health Sciences Center, West Virginia University, P.O. Box 9304, Morgantown, West Virginia 26506, United States

ABSTRACT: The appearance of neuritic amyloid plaques comprised of β-amyloid peptide (Aβ) in the brain is a predominant feature in Alzheimer's disease (AD). In the aggregation process, Aβ samples a variety of potentially toxic aggregate species, ranging from small oligomers to fibrils. Aβ has the ability to form a variety of morphologically distinct and stable amyloid fibrils. Commonly termed polymorphs, such distinct aggregate species may play a role in variations of AD pathology. It has been well documented that polymorphic aggregates of Aβ can be produced by changes in the chemical environment and peptide preparations. As Aβ and several of its aggregated forms are known to interact directly with lipid membranes and this interaction may play a role in a variety of potential toxic mechanisms associated with AD, we determine how different Aβ(1−40) preparation protocols that lead to distinct polymorphic fibril aggregates influence the interaction of Aβ(1−40) with model lipid membranes. Using three distinct protocols for preparing Aβ(1−40), the aggregate species formed in the absence and presence of a lipid bilayers were investigated using a variety of scanning probe microscopy techniques. The three preparations of Aβ(1−40) promoted distinct oligomeric and fibrillar aggregates in the absence of bilayers that formed at different rates. Despite these differences in aggregation properties, all Aβ(1−40) preparations were able to disrupt supported total brain lipid extract bilayers, altering the bilayer's morphological and mechanical properties.

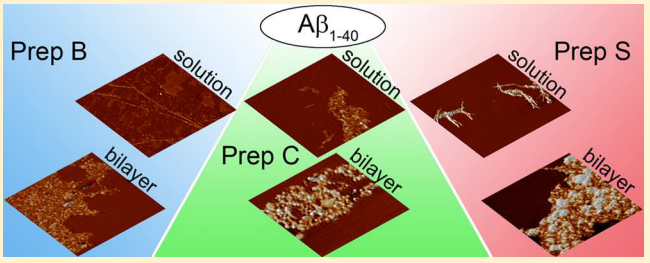

A common feature associated with several neurodegenerative diseases is the formation of extended, β-sheet rich, proteinaceous fibril aggregates, commonly termed amyloid.[1] Neuritic amyloid plaques composed predominately of aggregate forms of β-amyloid peptide (Aβ) are a major neuropathological hallmark of Alzheimer's disease (AD). The process of Aβ aggregation can be multifaceted and complex, with several metastable, intermediate species directly associated with fibril formation.[2,3] Similar to other amyloid-forming peptides, Aβ forms a variety of aggregates, including distinct oligomers and protofibrils.[4−7] Furthermore, Aβ can also aggregate into a variety of morphologically distinct fibril structures, termed polymorphs.[5,8,9] The polymorphic Aβ fibril structure depends on numerous environmental conditions during aggregation, and as a result, the protocol used to prepare Aβ for *in vitro* experiments directly determines Aβ fibril morphology.[8] While polymorphic aggregates are readily observed in *in vitro* studies, such structures are also detected in amyloid aggregates extracted from tissue, suggesting that a variety of distinct Aβ aggregate morphologies may play a role in AD.[10,11] For example, it has been proposed that polymorphic aggregates and fibrils may result in distinct biological activities and levels of toxicity.[12]

A potentially important contributing factor to the emergence of distinct polymorphic aggregates is the presence of cellular surfaces comprised predominately of lipids. The lipid bilayer environment associated with cellular membranes exerts an influence on protein structure and dynamic behavior, potentially acting in such a way to nucleate Aβ aggregation and/or promote the formation of specific Aβ aggregate species.[13] Importantly, model lipid membranes alter Aβ conformation and exert enormous influence on the aggregation state.[14−19] Beyond promoting Aβ aggregation,[20,21] cellular membranes may be directly damaged by Aβ aggregates and/or the aggregation process, causing membrane dysfunction because of perturbation of the bilayer structure and/or the formation of pores.[22−25] Lipids can promote and stabilize toxic Aβ protofibrils when the peptide has already aggregated into mature fibrils, providing another potential role for lipids in Aβ toxicity.[26]

Most studies of membrane-mediated Aβ aggregation have been performed with model systems, such as lipid vesicles or supported bilayers of varying composition, highlighting the

Received: June 26, 2014
Revised: October 25, 2014
Published: October 28, 2014

dx.doi.org/10.1021/bi500792f | *Biochemistry* 2014, 53, 7038−7050

importance of the chemical and physical properties of lipid membranes in the aggregation process.[27−35] As the ability of Aβ to form polymorphic aggregates depending on preparation (prep) conditions is well established, and the interaction between Aβ and lipid membranes may play a key role in several potential toxic mechanisms associated with AD, there is a need to understand how preparatory protocols of Aβ influence Aβ−lipid interactions. Herein, we determine how different preparation protocols of Aβ(1−40) that lead to polymorphic fibrils influence the interaction of Aβ(1−40) with model lipid membranes. Three distinct protocols for preparing Aβ(1−40) (Table 1) were used. These preparations varied in the method

Table 1. Aβ(1−40) Preparation and Incubation Conditions

prep	temp (°C)	buffer	monomer disaggregation	ref
B	24	phosphate	none	Kodali et al.[8]
C	24	PBS	HFIP/TFA	Kodali et al.[8]
S	24	PBS	HFIP/DMSO	Stine et al.[36]

of disaggregating stock lyophilized samples of Aβ(1−40) and final buffer conditions, and each preparation has been reported to produce unique aggregate structures.[8,36] We characterize the aggregates formed in free solution (in the absence of a bilayer) from these three different preparations of Aβ(1−40), verifying that they promote not only fibril polymorphs but also distinct oligomers. Then, we expose model total brain lipid extract (TBLE) bilayers to Aβ(1−40) prepared by these different protocols to determine their impact on the interaction of Aβ(1−40) with membranes.

MATERIALS AND METHODS

Aβ Peptide Preparation. Lyophilized, synthetic Aβ(1−40) (AnaSpec Inc., San Jose, CA) was prepared by three distinct protocols shown to result in the formation of distinct, polymorphic fibril aggregates. Preparations B and C were based on protocols published by Kodali et al. (also labeled B and C),[8] and preparation S was based on the work of Stine et al. (Table 1).[36] An initial disaggregation step was performed for prep C as follows: The lyophilized peptide was suspended in 1 mL of trifluoroacetic acid (TFA), sonicated for 10 min in a bath sonicator (VWR, model 75D) at 25 °C, and dried under a gentle stream of nitrogen to obtain a thin Aβ film. This film was dissolved in 1 mL of hexafluoroisopropanol (HFIP) and incubated at 37 °C for 1 h. The peptide was dried under a gentle stream of nitrogen. The new Aβ film was treated a second time with 2 mL of HFIP to ensure complete removal of the TFA and again dried under a nitrogen stream. The resulting peptide film was further dried under vacuum in a Vacufuge concentrator (Eppendorf) for 60 min. Fresh 2 mM NaOH (0.5 mL) was added to each tube and left to stand undisturbed for 5 min; 0.5 mL of 2× phosphate-buffered saline (PBS) (pH 7.3) with 0.1% sodium azide was slowly added to each sample without agitation. Each sample tube was centrifuged at 386000*g* overnight at 4 °C in an ultracentrifuge. After 24 h, the supernatant was carefully removed and the disaggregated peptide was snap-frozen in liquid nitrogen and stored at −80 °C. These frozen aliquots were thawed on ice, and the actual peptide concentration of the stock was determined using the Protein A280 assay of a NanoDrop spectrophotometer (Thermo Scientific). Then, a final dilution into PBS (pH 7.3) containing 0.05% (w/v) sodium azide to the desired final concentration of 20 μM for experiments was performed.

In prep B, there was no initial disaggregation step, and samples were prepared directly from the lyophilized Aβ stock. In short, 2 mM NaOH was added to the peptide, followed by sonication for 5 min in a bath sonicator (VWR, model 75D) at 25 °C, and measurement of the actual peptide concentration of the stock using the Protein A280 assay of a NanoDrop spectrophotometer (Thermo Scientific). Then, dilution to the desired final peptide concentration of 20 μM in 10 mM phosphate buffer (pH 7.4) and 0.05% (w/v) sodium azide for experiments was performed.

For prep S, Aβ(1−40) was treated with HFIP to dissolve seeds and preexisting aggregates within the lyophilized stock. The peptide sample was placed in a Vacufuge concentrator (Eppendorf) to remove all HFIP, resulting in a peptide film. To make a 2000 μM stock solution, the peptide film was dissolved in 10 μL of dimethyl sulfoxide (DMSO) at 37 °C and sonicated in a bath sonicator (VWR, model 75D) for 20 min at 25 °C, and the actual peptide concentration of the stock was measured using the Protein A280 assay of a NanoDrop spectrophotometer (Thermo Scientific). The stock solution was diluted into PBS buffer (pH 7.3) to obtain a final concentration of 20 μM. For aggregation assays in free solution, incubations of all three preps were maintained at 24 °C. For *in situ* AFM experiments, the final dilution to 20 μM was performed in the fluid cell for all three preps.

Thioflavin T (ThT) Aggregation Assay. A stock solution of 1 mg/mL ThT (Acros Organics) was prepared. Samples of Aβ(1−40) prep B, C, or S were prepared at 20 μM and incubated with 20 μM ThT at 24 °C in clear 96-microwell plates that were sealed to prevent evaporation. The ThT fluorescence was measured every 15 min for 60 h using a microplate reader (Molecular Devices, Sunnyvale, CA) with excitation and emission filters set at 440 and 480 nm, respectively, and a medium flash (six flashes/read). All ThT fluorescence assays were performed in triplicate, normalized, and plotted in arbitrary units (a.u.). ThT assay results were verified among four independently performed experiments.

Preparation of Supported Lipid Bilayers. At a concentration of 1 mg/mL, three different stock solutions of lyophilized porcine TBLE (Avanti Polar Lipids, Alabaster, AL) were made from the same lot of lipids. The buffers of the three stock solutions matched those associated with each Aβ prep. Each stock solution was treated similarly to prepare lipid vesicles. In short, bilayers and multilayer lipid sheets were formed by five cycles of freeze−thaw treatment using an acetone/dry ice bath,[18,19] and these lipid suspensions were sonicated for 15 min in a bath sonicator (VWR, model 75D) at 25 °C. Each buffer (15 μL) was injected directly into the AFM fluid cell, and via vesicle fusion, a 40 μm × 40 μm supported lipid bilayer was formed on freshly cleaved mica. Three washes with 15 μL of PBS were performed to remove excess lipid vesicles from the fluid cell once the bilayer was formed.

Atomic Force Microscopy (AFM) Imaging Conditions. For *ex situ* AFM imaging of dried samples, 2 μL aliquots of each Aβ incubation were spotted onto freshly cleaved mica for 30 s at various time points, washed with 200 μL of high-performance liquid chromatography grade water, and dried under a gentle stream of nitrogen. For each Aβ preparation, three separate incubations were performed, and each was sampled at various times for AFM analysis. Peptide aggregate depositions were imaged with a Nanoscope V MultiMode scanning probe microscope (Veeco, Santa Barbara, CA) operated in tapping mode and equipped with a closed-loop

dx.doi.org/10.1021/bi500792f | *Biochemistry* 2014, 53, 7038−7050

vertical engage J-scanner. Images were acquired with diving board-shaped silicon cantilevers with a nominal spring constant of 40 N/m, scan rates of 2−3 Hz, and a resonance frequency of ∼300 kHz.

In situ AFM experiments were also performed with a Nanoscope V MultiMode scanning probe microscope (Veeco) equipped with a fluid cell sealed with an O-ring and operated in tapping mode with scan rates of 1−2 Hz and cantilever drive frequencies of ∼8−10 kHz. *In situ* images were obtained with V-shaped oxide-sharpened silicon nitride cantilevers with a nominal spring constant of 0.5 N/m (Budget Sensors, Sofia, Bulgaria). Filtered buffer (35 μL), which matched each Aβ prep, was added to the fluid cell, and background images were obtained to ensure cleanliness of the cell before direct injection of 15 μL of a TBLE stock solution. Once formed, TBLE bilayers were exposed to each preparation of Aβ at a final concentration of 20 μM. Upon injection of Aβ, a 10 μm × 10 μm image of the surface with 1024 pixel × 1024 pixel resolution was taken before sealing the fluid cell to prevent evaporation. The bilayer was imaged again 4−8 and 16−20 h after exposure to Aβ(1−40).

Scanning Probe Acceleration Microscopy (SPAM) Imaging Conditions. Height images (10 μm × 2.5 μm) were captured with 512 pixel × 128 pixel resolution while simultaneously capturing the entire cantilever deflection signal for SPAM analysis.[37] Via a combination of a signal access module (Veeco) and a CompuScope 14100 data acquisition card (Gage, Lachine, QC), cantilever deflection trajectories were captured at 2.5 MS/s and 14 bit resolution with a vertical range of 2 V. A Fourier transform-based harmonic comb filter was applied to the deflection signal. To obtain the time-resolved tip acceleration, the second derivative of the filtered cantilever deflection (tip acceleration) was scaled by the effective mass (m_{eff}) of the cantilever to obtain the time-resolved imaging force associated with every tapping event during imaging. m_{eff} was determined using a thermal tuning method by obtaining the spring constant and resonance frequency of the cantilever.[38]

Quantitative Image Analysis. AFM image analysis was performed using MATLAB equipped with the image processing toolbox (MathWorks, Natick, MA) as described in greater detail by Burke et al.[39] In short, physical dimensions of Aβ aggregates were measured automatically from AFM images. AFM images were (1) imported into MATLAB, (2) flattened to correct for background curvature, and (3) converted into binary maps of aggregate locations using a height threshold set at 0.5 nm (assigning values of 1 to any image pixel that represented a height above the threshold and assigning a value of 0 to any pixel corresponding to a height below the threshold).[40] (4) Individual aggregates were located by looking for groupings of five or more pixels in the binary map that were equal to one using pattern recognition algorithms. (5) Specific features (height, volume, contour length, etc.) of each individual aggregate were measured by implementing the region property commands from the image processing toolbox in MATLAB and cross-referencing the binary map. Each detected aggregate was assigned an individual tracking number so that sorting into different types of aggregates (i.e., fibril or oligomer) based on measured dimensions could be verified by locating and labeling the aggregates identified by such filters. In this way, data sets were constructed that could be used to track thousands of individual aggregates and sort them on the basis of specific dimensional criteria.[39]

Analysis of the surface roughness and the percent area of bilayer disruption was performed as follows: (1) AFM images were imported into MATLAB. (2) Flattening was used to correct for background curvature. (3) Images were converted into binary maps using a height threshold set at 0.3 nm (an unperturbed bilayer has a roughness of ∼0.2 nm) in the same fashion as described above. (4) Because of the large variability of height within a region of the bilayer with a disrupted morphology, there are pixels associated with these regions that are smaller than the 0.3 nm threshold, which necessitated an additional step to include these pixels in further calculations. This was accomplished by applying a smoothing filter to the binary image that resulted from the initial application of the height threshold. (5) As image pixels associated with undisrupted and disrupted regions of the bilayer have now been identified by the binary image, the surface roughness of these regions can be calculated by determining the root-mean-square (rms) roughness of just those pixels associated with each type of region. Comparison of the rms roughness of undisrupted regions of bilayers exposed to Aβ with the rms roughness of bilayers that were not exposed to Aβ can act as an internal control. The percent area of the bilayer disrupted can be calculated by determining the fraction of pixels assigned a value of 1 in the binary image.

RESULTS

Different Aβ(1−40) Preparation Protocols Alter Aggregation Kinetics and Aggregate Morphology. To compare the aggregation of Aβ(1−40) prepared by the three different protocols and verify the formation of polymorphic aggregates, we performed a combination of ThT aggregation assays and AFM analysis of aggregate morphology under free solution aggregation conditions (defined as no surface or lipid present during incubation). Aggregation that occurred in solution in the absence of any lipid surface will be termed to occur in "free" solution. That is, these aggregation reactions occurred free from the presence of any lipid surfaces. Three distinct 20 μM Aβ(1−40) solutions were prepared via the corresponding protocol as described in Materials and Methods and Table 1, and the aggregation kinetics of preps B, C, and S were analyzed by a ThT assay (Figure 1). While Aβ(1−40) prepared by the three different protocols displayed the characteristic lag and growth phases traditionally associated with amyloid formation, the apparent rates associated with

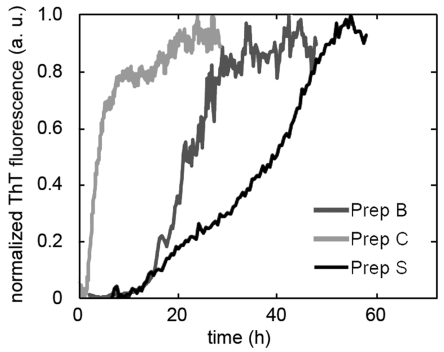

Figure 1. ThT analysis of the aggregation of Aβ(1−40) prepared by the three different protocols, B, C, or S. Curves were normalized to the maximal value of fluorescence. Each curve represents the average of triplicate measurements performed on a single 96-microwell plate, but the results were reproduced in a total of four experiments.

dx.doi.org/10.1021/bi500792f | *Biochemistry* 2014, 53, 7038−7050

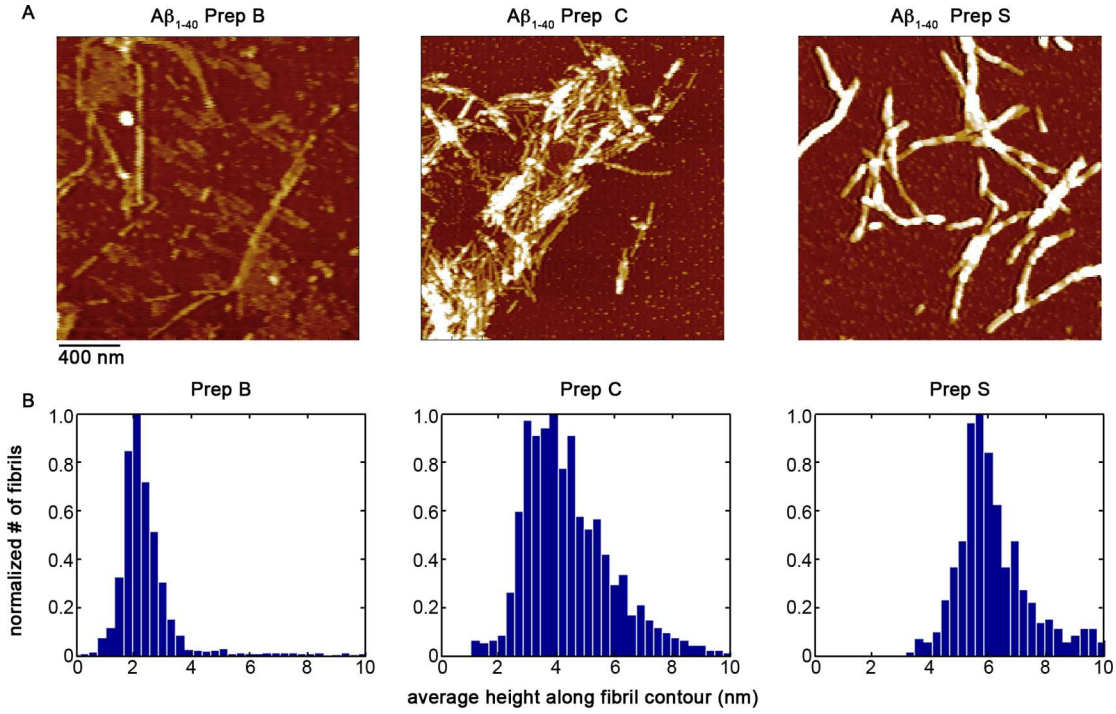

Figure 2. Three preparatory protocols for Aβ(1−40) resulted in polymorphic fibril aggregates in free solution. (A) Representative *ex situ* AFM images of fibrils formed by Aβ(1−40) prepared by protocol B, C, or S. Samples were taken at time points corresponding to the post-growth phase steady state condition indicated by ThT (Figure 1) for each preparation. The scale bar is applicable to all images. (B) Histograms of the average heights along the fibril contour for fibrils formed by each preparation. Data presented here for each preparation were compiled from several images from three independent replicates of the aggregation experiment.

these phases varied across preparations. Prep C had the shortest lag phase (∼1.5−2 h), followed by prep B and prep S with lag phases of ∼15−16 and ∼17−18 h, respectively. All three preparations of Aβ(1−40) then underwent a growth phase that eventually reached a steady state ThT fluorescence level. Of the three preparations, prep S appeared to have the slowest growth phase. It is surprising that prep C, which involved the most extensive disaggregation procedures, has the shortest lag phase. A potential explanation for this is that the snap-freezing and subsequent thawing of the resulting stock solution of Aβ(1−40) prepared by prep C result in the re-formation of some seeds. Importantly for this study, there were still an observed lag phase, growth phase, and steady state phase from which we could sample for analysis of fibril and oligomer morphology.

Incubations of Aβ(1−40) prepared by each protocol were sampled and deposited on a mica substrate at a time point after the growth phase had reached steady state (based on the ThT assay) for AFM analysis of the resulting fibril aggregates. On the basis of these images, the three Aβ preparation protocols indeed promoted the formation of distinct Aβ fibril polymorphs when they were incubated in free solution (Figure 2). Image analysis was performed to investigate the morphological differences of fibrils associated with each Aβ(1−40) preparation. For this analysis, only features taller than 0.5 nm with an aspect ratio (aggregate length divided by width) of >3 were defined as fibrils. The ability of such criteria to successfully distinguish fibrils from AFM images has been previously established.[39] As the height can vary along the length of a fibril, the average height (or thickness perpendicular to the long axis of the fibril) along the contour of each fibril was determined. The distribution of this average height varied for fibrils associated with each Aβ preparation (Figure 2B). The results of this analysis (average, mode, and median of the measured heights) are summarized in Table 2. Prep B formed thin, relatively smooth fibrils with an average height of 2.0 ± 0.5 nm, which corresponds well to the mode and median of the distribution. Prep C fibrils had a stronger propensity to accumulate into large bundles, but individual fibrils were approximately twice as large compared to those from prep B on average. This average height of prep C is slightly larger than the mode because of the distribution of fibrils being skewed to larger values of height. Prep S resulted in the thickest fibrils with an average height and mode roughly 3 times larger than those of fibrils of prep B. Fibrils formed by prep S were often entangled and displayed the largest variation in height, as their morphology often had periodic features along their contours. Visual morphological inspection combined with these average height measurements confirmed that distinct, polymorphic fibrils were formed by the three different Aβ(1−40) preparation protocols.

Table 2. Height Measurements of Fibrils Associated with Each Preparation Protocol (aggregation in solution)

prep	mean ± STD (nm)	mode (nm)	median (nm)
B	2.0 ± 0.5	1.75−2.25	2.1
C	4.4 ± 1.6	2.15−4.25	4.2
S	6.3 ± 1.2	5.5−6.5	5.9

While it was clear that the late stage fibril aggregates associated with each preparation were indeed polymorphs, we next wanted to determine if distinct oligomeric precursors were also formed in free solution. For this analysis, aliquots were taken from the different Aβ(1−40) incubations at time points corresponding to the initial stages of the growth phase as

dx.doi.org/10.1021/bi500792f | *Biochemistry* 2014, 53, 7038−7050

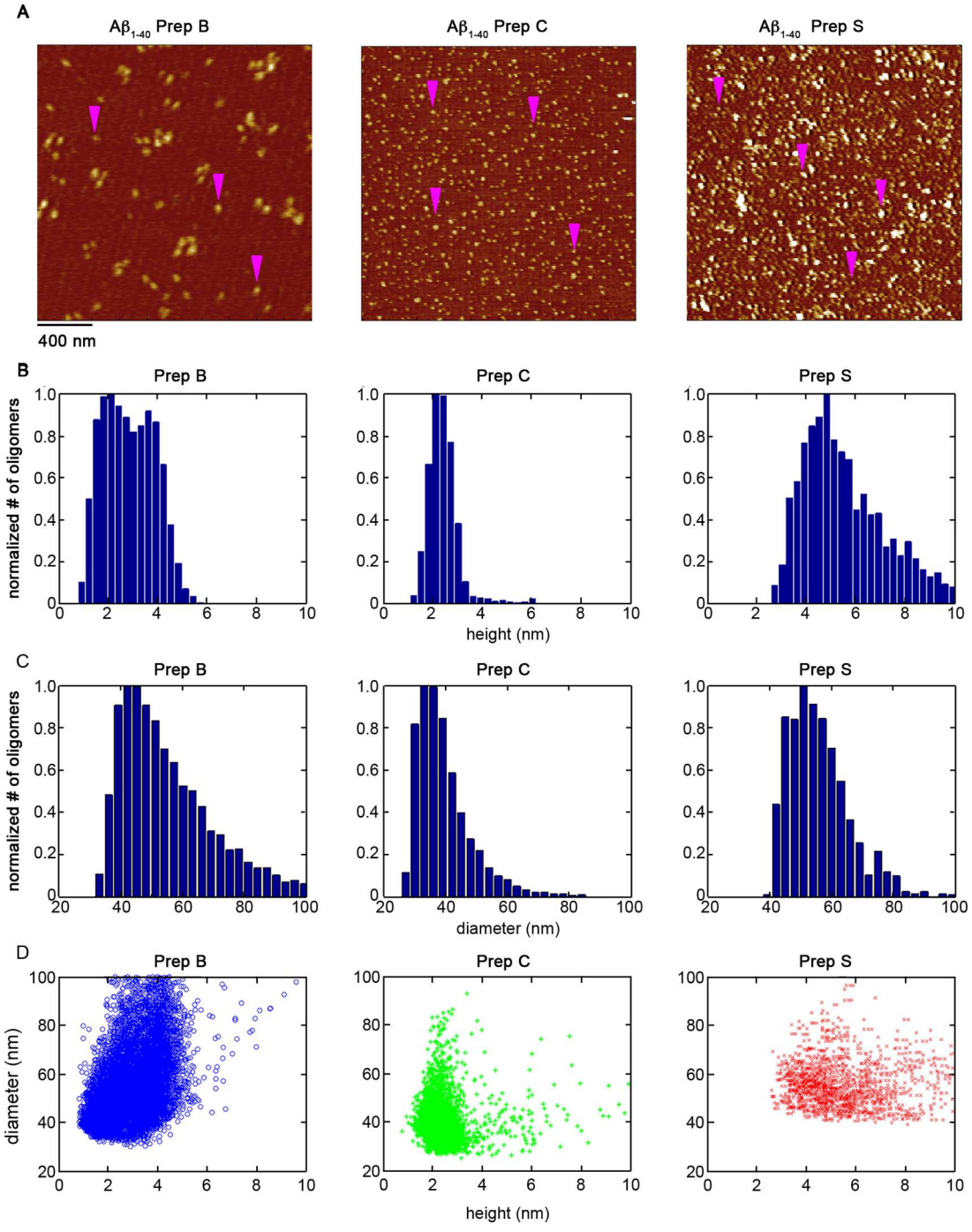

Figure 3. Three preparatory protocols for Aβ(1−40) resulted in distinct oligomeric aggregate populations in free solution. (A) Representative *ex situ* AFM images of globular, oligomeric aggregates formed by the different Aβ(1−40) prepared by protocol B, C, or S. Samples were taken during the growth phase indicated by ThT (Figure 1) for each preparation. The scale bar is applicable to all images. Oligomers are indicated by pink arrows. (B) Height and (C) diameter histograms of oligomers formed by each preparation. (D) Correlation plots of oligomer height vs diameter. Data presented here for each preparation were compiled from several images from three independent replicates of the aggregation experiment.

Table 3. Height and Diameter Measurements of Oligomers Associated with Each Preparation Protocol (aggregation in solution)

	height			diameter		
prep	mean ± STD (nm)	mode (nm)	median (nm)	mean ± STD (nm)	mode (nm)	median (nm)
B	2.9 ± 1.3	2.0−4.0	2.8	57.1 ± 20.1	37−45	51.0
C	2.5 ± 0.8	2.0−2.5	2.3	40.3 ± 14.5	30−40	37.5
S	6.5 ± 3.3	4.0−5.3	5.5	61.7 ± 27.6	42−58	55.1

dx.doi.org/10.1021/bi500792f | *Biochemistry* 2014, 53, 7038−7050

assessed by the ThT assay. These aliqouts were deposited on mica, dried, and imaged with AFM for analysis (Figure 3). Each Aβ preparation formed oligomers (Figure 3A). To distinguish oligomers from fibrils that may also be present in some of the images, oligomers were defined as features taller than 0.5 nm with an aspect ratio of <3, indicating a globular, circular structure. The ability of such criteria to successfully distinguish oligomers from fibrils in AFM images has been demonstrated.[39] The height and diameter of individual oligomers were measured, and the averages of these measurements are listed in Table 3. Because of the globular morphology associated with oligomers, the height was defined as the tallest image pixel contained within the aggregate structure. Analysis of oligomer heights (Figure 3B) and diameters (Figure 3C) indicated that the three Aβ(1−40) sample preparations also led to distinct oligomeric aggregates. While the average height of oligomers formed by prep B was 2.9 ± 1.3 nm, the height distribution appears to be slightly bimodal, suggesting that there may be two populations of oligomers associated with this prep. In prep B, there appears to be a population at ∼1.75−2.25 nm and another at ∼3.5−4.0 nm; however, the overall mode of the height distribution encompasses this entire range. There is no clear indication of a bimodal distribution of measured diameters of prep B oligomers. However, there is a pronounced tail in the diameter distribution of prep B oligomers, suggesting that perhaps the lateral resolution of AFM, which is limited by the finite size of the probe, was not able to resolve these two potential populations. In contrast, the height distribution of prep C Aβ(1−40) oligomers was quite sharp, with an average height of 2.5 ± 0.8 nm with a mode of ∼2.0−2.5 nm. The prep C oligomers also had the smallest average diameter. Oligomers associated with prep S were larger than the oligomers of the other two preps. There was also a significant population of larger oligomers (taller than 6 nm) observed for prep S. The distinct morphologies associated with oligomers of each preparation can be visualized by correlation plots of the height versus diameter of each individually measured oligomer (Figure 3D). It should also be noted that the diameter measurements are inflated because of the finite size of the AFM probe, and the reported numbers are not corrected for this contribution.

The observed sizes of these different oligomeric species are similar to those of Aβ aggregates observed by AFM in the literature. Aβ-derived diffusible ligands (ADDLs) range from 5 to 6 nm in height,[6] and spherical Aβ aggregates termed globulomers are 4−5 nm in height.[41] Both of these reported aggregate species are similar in size to the oligomers associated with prep S in this study. Smaller oligomers observed for preps B and C are similar to a smaller subset of globulomers that have been reported to range from 1 to 2 nm in height.[41] However, it should be noted that, on the basis of height, oligomers observed in this study are most likely larger than dodecamers, as the dodecamer Aβ*56 was shown to be only ∼1 nm in height.[42]

Aβ(1−40) Prepared by Different Protocols All Disrupt Lipid Bilayer Morphology. To determine how the preparation history of Aβ(1−40) affected its interaction with membranes, supported TBLE bilayers were systematically exposed to 20 μM solutions of Aβ(1−40) prepared by the three different protocols and imaged in solution using AFM. TBLE bilayers contain a physiologically relevant mix of lipid components (i.e., cholesterol, sphingolipids, isoprenoids, gangliosides, and both acidic and neutral phospholipids), and several properties of supported lipid bilayers are known to closely mimic those of free membranes.[43,44] Unperturbed TBLE bilayers appear to be smooth when they are imaged by AFM in solution and are stable for at least 24 h. The Aβ peptide was directly injected into the AFM fluid cell, and an image was taken immediately to ensure that the injection process did not damage the lipid bilayer. At 20 μM Aβ, no detectable alterations in the bilayer morphology or protein aggregates were observed within 4−6 h of exposure to each preparation of Aβ(1−40). Furthermore, continuous imaging of the bilayer appeared to interfere with the interaction between Aβ(1−40) and the supported bilayer. Therefore, the tip was disengaged from the bilayer surface, and we waited 16 h to resume imaging of the surface to provide sufficient time for the peptide to interact with the bilayer. AFM images were then collected at time points corresponding to 16−20 h after the initial exposure to the different preparations of Aβ(1−40).

After being exposed for 16 h, regions of increased surface roughness were observed on the supported bilayer for all three preparations of Aβ(1−40) (Figure 4). These regions contained

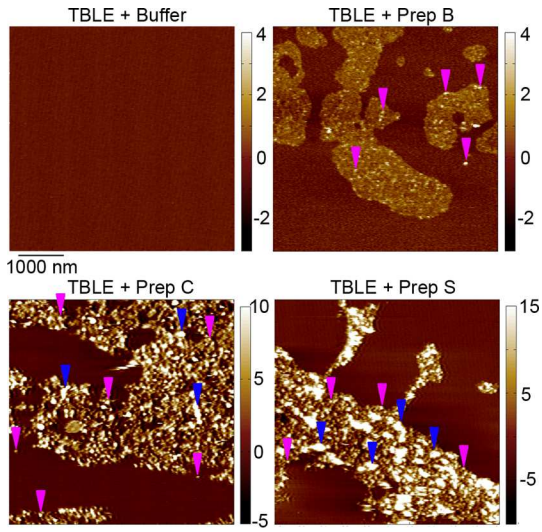

Figure 4. Representative *in situ* AFM images of supported bilayers after their exposure for 16−20 h to neat buffer (TBLE + buffer) or Aβ(1−40) prepared by protocol B, C, or S. The scale bar is for all AFM images. Note that the color scheme for each image is different. Arrows indicate oligomeric (pink) or amorphous (blue) aggregates.

what appeared to be Aβ(1−40) aggregates. For prep B, these aggregates were predominately oligomeric; however, for preps C and S, much larger amorphous aggregates were also observed. To determine the extent of interaction of each distinct Aβ(1−40) preparation with the bilayer, the percent surface area of the bilayer disrupted by Aβ(1−40) and the surface roughness of the disrupted regions were calculated using imaging processing software (Figure 5). After exposure for 16 h, the fraction of the bilayer surface area that was disrupted by each preparation was similar in magnitude, with preps B, C, and S disrupting 47.9 ± 4.6, 50.5 ± 5.9, and 50.5 ± 3.3% of the bilayer surface, respectively. While the area of the bilayer disrupted by Aβ(1−40) for preps B, C, and S was similar, the observed rms roughness within the disrupted regions varied with the Aβ preps. A freshly formed, unperturbed TBLE bilayer had a rms surface roughness of 0.22 ± 0.07 nm (Figure 5B). The rms roughness measurements of the regions of disrupted bilayer morphology were restricted to those regions, and pixels associated with Aβ aggregates were removed from the analysis to avoid bias due to variations in the

dx.doi.org/10.1021/bi500792f | *Biochemistry* 2014, 53, 7038−7050

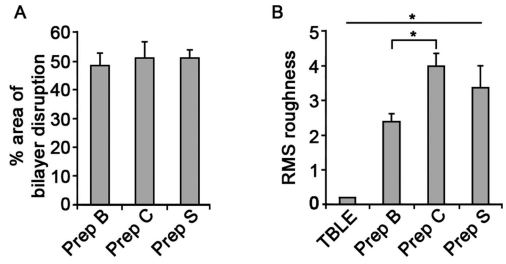

Figure 5. Quantification of lipid bilayer roughening. (A) Percent area of TBLE bilayers containing increased roughness induced by Aβ(1−40) prepared by the different protocols. The area of the bilayer affected by exposure to Aβ(1−40) prepared by the distinct protocols was not significantly different. (B) rms roughness analysis of regions of the bilayer disrupted by Aβ(1−40) prepared by the different protocols. All three preparations of Aβ(1−40) significantly roughened the bilayer compared to TBLE bilayers that had not been exposed to any peptide. However, the rms roughness associated with exposure to preparations C and S was significantly larger than that associated with prep B (*p < 0.01). Data presented here for each preparation were compiled from several images from at least three separate experiments.

number of aggregates within a region. Each Aβ preparation induced significant (p < 0.01) bilayer roughening when compared to undisturbed TBLE as assessed by a t test. Prep B had an increased surface roughness of 2.41 ± 0.18 nm, which was significantly smaller than the roughness associated with preps C and S. Prep C induced a rms surface roughness of 4.00 ± 0.32 nm in the bilayer, and prep S caused an increased rms surface roughness of 3.39 ± 0.60 nm. This greater induced magnitude of surface roughening may potentially be associated with the formation of the larger amorphous aggregates observed for both preps C and S, but not prep B.

Next, we analyzed the size of the Aβ(1−40) aggregates observed on the supported bilayers to determine if these preps still resulted in distinct aggregates in the presence of the lipid and/or if the lipid altered the type of aggregates formed. As there were no clear fibrils observed to form on the bilayer in the experimentally accessible time frame associated with the AFM experiments on lipid bilayers, we were unable to assess if fibril structure was altered on the membrane surface. We were, however, able to analyze oligomers that formed in the presence of the lipid bilayers (Figure 6 and Table 4). In an analysis of the size of oligomers and other aggregates observed on the TBLE bilayers, it is important to note a few caveats that are applicable

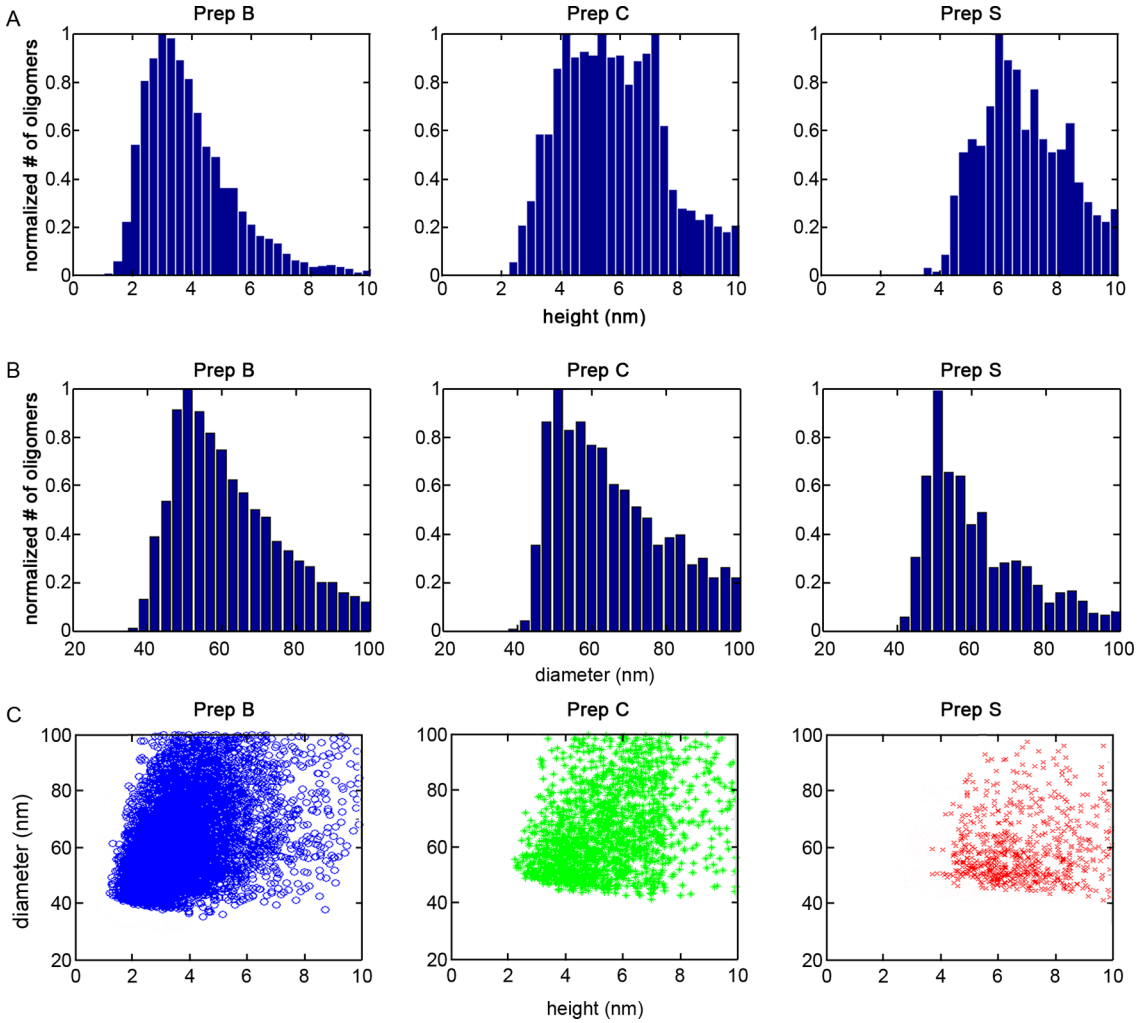

Figure 6. Morphological analysis of oligomers formed by Aβ(1−40) prepared by protocol B, C, or S in the presence of total brain lipid extract bilayers. (A) Height and (B) diameter histograms of oligomers formed by each preparation in the presence of lipid bilayers. (C) Correlation plots of oligomer height vs diameter. Data presented here for each preparation were compiled from several images from at least three separate experiments.

dx.doi.org/10.1021/bi500792f | *Biochemistry* 2014, 53, 7038−7050

Table 4. Height and Diameter Measurements of Oligomers Associated with Each Preparation Protocol (aggregation on bilayer)

	height			diameter		
prep	mean ± STD (nm)	mode (nm)	median (nm)	mean ± STD (nm)	mode (nm)	median (nm)
B	4.1 ± 1.5	3.0–3.75	3.9	63.0 ± 14.4	50–65	63.3
C	5.8 ± 1.7	4.0–7.5	6.4	66.6 ± 14.2	45–70	67.4
S	6.7 ± 1.4	4.0–5.3	7.6	62.0 ± 25.6	50–60	58.7

to all Aβ(1–40) preps. First, in the AFM images, there is no way to determine if the aggregate is comprised completely of peptide or if there are some lipid components incorporated into the structure. The possibility that lipid components are included in the observed aggregates is reasonable considering that lipid components are found in neuritic plaques and inclusions.[45,46] Second, we are able to analyze only the aggregate structure protruding above the lipid bilayer. As the aggregate may be partially inserted into the bilayer, the actual size of the aggregate may be underestimated. Finally, as AFM can image features only on the surface, we cannot determine if the aggregate formed on the bilayer surface or in the solution above the bilayer before being deposited on the surface.

Oligomers observed on the bilayer associated with prep B were on average (Figure 6 and Table 4) larger than those observed to form in the absence of the bilayer under the same respective preparatory conditions (Figure 3). Furthermore, there was no indication of a bimodal distribution in height of prep B oligomers on the bilayer, and the mode of this height distribution fell between the two observed modes of prep B oligomers formed in free solution. While no oligomers larger than 6 nm in height were observed for prep B incubations in free solution, such larger oligomers were commonly observed on the bilayer. While there is considerable overlap between the height versus diameter correlation plots of prep B oligomers formed in the presence and absence of bilayers, the variation in oligomer size is much more pronounced in the presence of the bilayer. This analysis indicates that prep B oligomers formed in the presence of the bilayer have a more heterogeneous distribution of size and morphology.

In a comparison of the oligomers formed from prep C in the absence (Figure 3 and Table 3) and presence of bilayers (Figure 6 and Table 4), there is a significant shift to much larger aggregate species observed on the bilayer. While the height mode of prep C oligomers formed in free solution was ~2.0–2.5 with few oligomers larger than 4 nm, there were minimal oligomers observed that were smaller than 3.0 nm on the bilayer, and there was a large, heterogeneous population of oligomers ranging from 4 to 7.5 nm in height. A significant population of prep C oligomers larger than 8 nm in height was also observed on the bilayer. While the majority of oligomers formed in free solution from prep C were smaller than 40 nm in diameter, the distribution of oligomer diameters starts at ~40 nm on the bilayer. Comparison of the height versus diameter correlation plots associated with prep C oligomers formed in the absence or presence of lipid bilayers suggests that the lipid membrane promotes the formation of a distinct population of larger oligomers for this preparation protocol.

While the distributions of oligomer size observed on the bilayer with prep S (Figure 6 and Table 4) were similar to those observed in the absence of bilayer (Figure 3 and Table 3), the oligomers on the bilayer were skewed slightly larger to their free solution counterparts. For prep S, there was also significant overlap in the height versus diameter correlation plots between oligomers formed in the absence or presence of bilayers. On the basis of morphology alone, it is not apparent that these oligomers appearing on the bilayer with prep S are different from their free solution counterparts.

While not observed in appreciable numbers for prep B, there were a significant number of larger, amorphous aggregates formed by prep C and prep S in the presence of the lipid bilayer (Figures 4 and 7). Similar amorphous aggregates were not

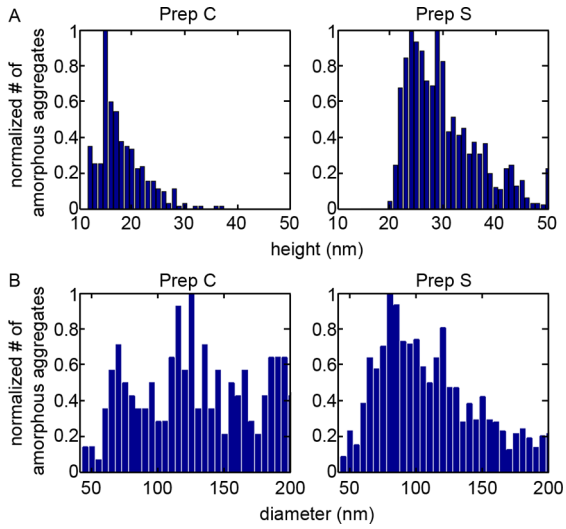

Figure 7. Morphological analysis of amorphous aggregates formed by Aβ(1–40) prepared by protocol C or S in the presence of total brain lipid extract bilayers. (A) Height and (B) diameter histograms of oligomers formed by each preparation in the presence of lipid bilayers are presented. Data presented here for each preparation were compiled from several images from at least three separate experiments.

present in AFM images of aggregates formed in free solution. We are terming these structures amorphous aggregates for several reasons. (1) Their height above the bilayer is significantly larger than those of other aggregate types observed, and (2) they do not have an obviously globular or fibrillar morphology as they had a bumpy, clumpy appearance. It is possible that these amorphous structures represent accumulations of smaller aggregate structures. These amorphous aggregates were observed only in regions of the supported bilayers that displayed increased surface roughness. Because of their unique morphology, amorphous aggregates typically had aspect ratios of >3, and thus, they could be systematically identified in images to construct height and diameter histograms (Figure 7). The amorphous aggregates formed by prep C were typically smaller in height than those of prep S, with average values of 17.8 ± 5.5 and 29.2 ± 6.5 nm, respectively. Despite being shorter, the amorphous aggregates of prep C often were larger in the lateral dimension than their prep S counterparts (Figure 7B); however, amorphous aggregates for both preps were highly heterogeneous, without a clear mode in size.

dx.doi.org/10.1021/bi500792f | Biochemistry 2014, 53, 7038–7050

Aβ Prepared by Different Protocols Induce Similar Mechanical Changes in Lipid Bilayers. As all of the Aβ(1−40) preparations altered the morphology of the supported lipid bilayers, we next determined the mechanical impact of these changes associated with exposure to Aβ(1−40). To accomplish this, SPAM, which recovers the time-resolved tip/sample force associated with every tapping event during the acquisition of a tapping mode AFM image taken in solution, was used.[37] Specific features of these time-resolved tip/sample forces, the maximal tapping force (F_{max}) and minimal tapping force (F_{min}) per oscillation cycle, are sensitive to the mechanical properties of the surface and can be used to map relative changes in such properties along a surface with a high spatial resolution.[28,47,48] F_{max} refers to the peak or largest repulsive (positive) force between the tip and surface associated with an individual tapping event, and F_{min} is the largest magnitude attractive (negative) force experienced during a tapping event. Several numerical simulations and experimental studies have demonstrated that F_{max} can be directly related to the compression modulus of the surface and that F_{min} is sensitive to the adhesive interaction between the tip and surface.[28,47,48] As the force data are taken simultaneously during standard tapping mode AFM imaging in solution, changes in imaging forces can be directly correlated with topographical features of the surface. Because of difficulties in controlling for variations in cantilever properties and imaging parameters between individual experiments, SPAM is currently limited to measuring relative, spatial differences in surface mechanical properties within a single image. For example, larger cantilever spring constants result in larger values of F_{max}, but for any given spring constant (or any individual cantilever), the relative magnitude of F_{max} reflects the surface's compression modulus.[28,47−49] That is, the magnitude of F_{max} increases with increasing surface rigidity with a power law dependence.[28,47,48] Despite being limited to making comparisons within a single experiment, we have determined the morphological and mechanical changes associated with exposing lipid bilayers to the different preparations of Aβ(1−40). It should be noted that the disrupted regions of the bilayer contain a heterogeneous mixture of lipids, peptides, and aggregates. As a result, the observed changes in mechanical properties associated with these regions arise from this complex mixture.

Both F_{min} and F_{max} images of bilayers exposed to any of the three Aβ(1−40) preparations displayed a distinct contrast between the undisturbed regions of the bilayer and the disrupted regions of the bilayer (Figure 8). Histograms of F_{min} and F_{max} for every tapping event can be sorted on the basis of topography, allowing each tapping event to be associated with specific regions of the bilayer. The domains in which Aβ(1−40) interacted with lipid, resulting in a perturbed membrane morphology, were associated with smaller magnitudes of both F_{min} and F_{max} compared to those of the undisturbed lipid domains. There are several implications of these changes in the tip/sample force interaction associated with disrupted regions of the bilayer. The observed decreases in the magnitude of F_{min} associated with disrupted regions of the bilayer are primarily due to a weakened adhesive interaction between the disrupted bilayer and the AFM tip.[28,47,48] The observed decrease in the magnitude of F_{max} associated with disrupted regions of the bilayer indicates a decreased membrane rigidity or compression modulus.[28,47,48] Collectively, these results indicate that interaction between lipid bilayers and Aβ(1−40), independent of the preparatory history, results in regions of altered membrane morphology (increased roughness) and mechanical properties (decreased compression modulus of the bilayer and a weakened adhesive interaction between the tip and surface). One explanation for this observed impact on the bilayer due to exposure to Aβ(1−40) is a decrease in the efficiency of the packing of the lipid components within the bilayer in response to protein insertion or binding and aggregation, leading to a roughened morphology that would be more compressible.

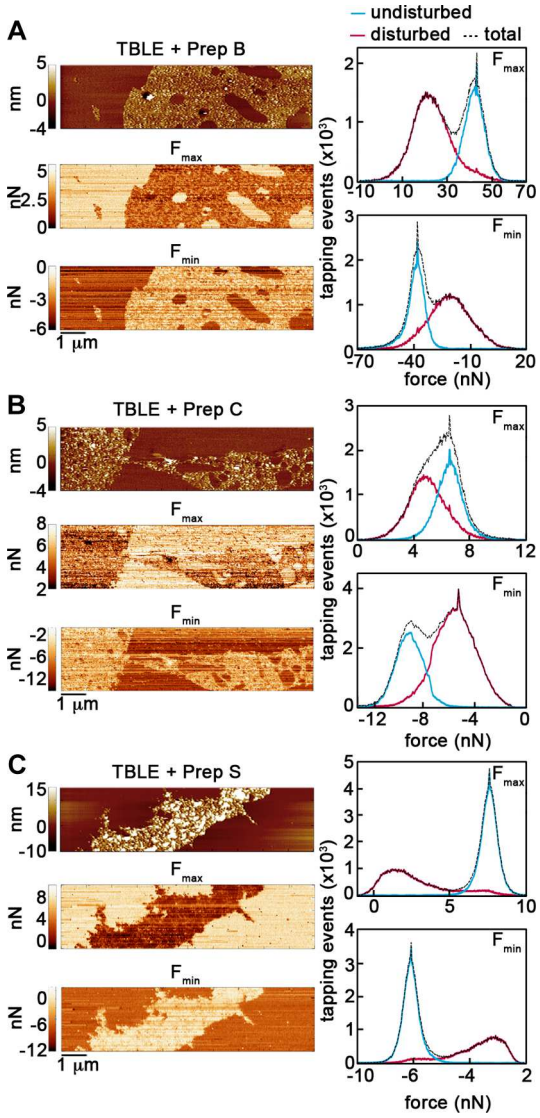

Figure 8. Topography, F_{max}, and F_{min} images of TBLE bilayers exposed to Aβ(1−40) prepared from (A) protocol B, (B) protocol C, or (C) protocol S, obtained using SPAM. Histograms of F_{max} and F_{min} for every tapping event associated with obtaining the images are presented at the right. The forces in each histogram were sorted on the basis of their association with disrupted or undisrupted regions of the bilayer as assessed by the corresponding AFM topography image.

DISCUSSION

While the *in vitro* aggregation of Aβ has been extensively studied, the existence of polymorphic aggregate structures is an inherent property of Aβ fibril formation.[5,8,9,50−52] In this study, various preparation protocols for Aβ(1−40) that are known to result in the formation of fibril polymorphs were used to determine the impact of the prep on the interaction of Aβ(1−

dx.doi.org/10.1021/bi500792f | *Biochemistry* 2014, 53, 7038−7050

40) with lipid membranes. Beyond confirming that preps B, C, and S promote fibril polymorphs in the absence of lipid bilayers, we also demonstrated that distinct oligomeric aggregates were associated with each preparation protocol in free solution. Furthermore, freshly prepared solutions of Aβ(1−40) of each prep were able to bind, disrupt, and alter the mechanical properties of lipid bilayers. While the extent of bilayer disruption was similar upon exposure to each Aβ(1−40) preparation, aggregates of Aβ(1−40) observed on the bilayer were distinct from their free solution counterparts in terms of morphology, suggesting that the presence of lipids can further modulate the aggregation process.

The ability to form polymorphic fibrils is an established property of Aβ.[5,8,9,50−53] This phenomenon can be attributed to several factors, including distinct nucleation events, thermodynamic stability of a variety of amyloid structures, and low dissociation rates associated with monomers from fibrils.[54] As suggested in this and other studies, Aβ can also form a variety of oligomeric species that may be on or off the pathway to fibril formation.[4,55,56] Furthermore, computational studies indicate that Aβ fragments under physiological conditions exist as an ensemble of a variety of polymorphs.[57] With the vast heterogeneity in potential Aβ aggregate structures, it has been a daunting task in the AD field to identify species that are the most relevant to neurodegeneration. Ultimately, structural variations of Aβ aggregates within the brain may be biomedically relevant. This notion is supported by observations that fibril polymorphs are toxic to neuronal cell cultures to varying degrees.[12] While there is mounting evidence that a variety of Aβ oligomers are neurotoxic,[42,58−61] mature fibrils have also been shown to induce toxicity in cell cultures.[12,62−64] Interestingly, Aβ aggregates purified from two AD patients' brains were able to seed the formation of Aβ(1−40) fibrils *in vitro*, resulting in distinct fibril polymorphs associated with each patient and further supporting the notion that polymorphic aggregates exist *in vivo*.[11] Furthermore, the Aβ(1−40) fibrils derived from these two patients were not polymorphic, suggesting that the majority of fibrils in each patient arose from nucleation of a specific polymorphic structure at a single site.[11]

Collectively, this suggests that there may be multiple toxic species that can result in AD pathology and that not all of these species are required to develop AD. Our study demonstrates that, despite being prepared with different protocols that promote distinct polymorphic oligomers and fibrils, Aβ(1−40) retains an ability to alter lipid membranes. If multiple, distinct species of Aβ are involved in AD, then therapies aimed at specific aggregates may not be effective, and targeting Aβ further upstream in the aggregation process may be justified. Furthermore, the presence of lipid further modulated Aβ(1−40) aggregate structure, consistent with reports that lipid membranes lead to conformational changes in Aβ.[30] This could also impact therapeutic strategies aimed at altering peptide aggregation. Such a scenario has been demonstrated experimentally as (−)-epigallocatechin gallate (EGCG), known to inhibit the aggregation of several amyloid-forming proteins,[65,66] was ineffective at inhibiting aggregation of human islet amyloid polypeptide (h-IAPP) in the presence of phospholipid membranes.[67]

While the ability of Aβ(1−40) to bind membranes was independent of preparatory history, once bound, each prep of Aβ(1−40) perturbed bilayer morphology. Exposure to each Aβ prep resulted in regions of increased surface roughness that were associated with a softer compression modulus and a reduced level of adhesion to the AFM probe tip compared to those of unperturbed regions of the bilayer. Collectively, these results suggest that Aβ(1−40) prepared from a variety of protocols, and presumably with different aggregation profiles as a result, can negatively impact the mechanical integrity of lipid membranes. A plausible explanation for the bilayer roughening and mechanical changes is that lipid molecules are displaced from their typical packing structure to accommodate Aβ binding and subsequent aggregation. NMR studies have suggested that exposure to Aβ indeed induces packing disorder in model bilayers,[27,29,68] and exposure to Aβ reduces the force necessary to puncture lipid membranes.[32] Beyond the change in compression modulus and adhesion properties observed here, Aβ can alter the fluidity of model lipid membranes,[69] which may also be related to an increased level of packing disorder. The ability of amyloid-forming proteins to disrupt membrane integrity and mechanical properties may represent a common mechanism leading to membrane dysfunction in amyloid diseases.[28] In this regard, computational studies using coarse-grained molecular dynamics in implicit solvent demonstrated not only that the aggregate structure of model amyloid peptides is modulated by lipids but also that the presence of these aggregates alters membrane structure locally, leading to altered mechanical properties of the membrane.[70]

On the basis of the observations that aggregate morphology observed for each prep on the bilayer was distinct compared to the morphology of the aggregates formed in free solution, the different time scales associated with observing oligomer formation on the bilayer compared with free solution, the absence of the formation of fibrils on the bilayer, and the appearance of larger amorphous aggregates was correlated with a significantly larger magnitude of surface roughness, this roughening of the bilayer may be associated with Aβ(1−40) aggregation occurring at the membrane surface. The ability of the presence of surfaces (including lipid bilayers) to alter the aggregation of Aβ is well-established, and such a notion is also consistent with the actual aggregation process being required for neurotoxicity.[71] However, as our observations are limited to those occurring on the bilayer surface, the possibility that the observed aggregates form in solution prior to binding the lipid bilayer cannot be ruled out.

The ability to use preformed aggregate seeds to circumvent the lag phase of Aβ aggregation and promote the formation of specific fibril polymorphs is well-established.[72−75] This ability of structurally variant Aβ aggregates to act as seeds is strikingly similar to the "strain" phenomenon associated with prion diseases in which distinct aberrantly structured prion aggregates promote their self-propagation within brain tissue.[76,77] Such a phenomenon may be active in neuron to neuron propagation of Aβ aggregate species.[78] In this regard, acceleration of AD occurs in transgenic mice upon injection of preformed Aβ aggregates, but this ability is dependent on the source of the exogenous Aβ.[76,79,80] While limited to just three preparatory protocols, our study demonstrates that differences in preparatory protocol leading to distinct Aβ fibril polymorphs do not inhibit the ability of Aβ(1−40) to aggregate on lipid membranes, and the presence of lipids actually influences the aggregation process. This suggests that a variety of Aβ structures that emerge early in the aggregation process can similarly interact with lipid membranes, which may play a role in stabilizing, promoting, or trafficking potential Aβ seeds.

AUTHOR INFORMATION

Corresponding Author

*Address: 217 Clark Hall, The C. Eugene Bennett Department of Chemistry, West Virginia University, Morgantown, WV 26505. E-mail: justin.legleiter@mail.wvu.edu. Telephone: (304) 293-0175.

Present Address

‖E.A.Y.: Chemistry Department, United States Naval Academy, 572 M Holloway Road, Annapolis, MD 21402.

Funding

This work was funded by the National Science Foundation (Grant 1054211) and the Alzheimer's Association (Grant NIRG-11-203834).

Notes

The authors declare no competing financial interest.

ABBREVIATIONS

Aβ, β-amyloid; AFM, atomic force microscopy; AD, Alzheimer's disease; DMSO, dimethyl sulfoxide; EGCG, (−)-epigallocatechin gallate; HFIP, hexafluoroisopropanol; h-IAPP, human islet amyloid polypeptide; m_{eff}, effective mass of the cantilever; NMR, nuclear magnetic resonance; PBS, phosphate-buffered saline; rms, root-mean-square; SPAM, scanning probe acceleration microscopy; STD, standard deviation; TBLE, total brain lipid extract; ThT, thioflavin T; TFA, trifluoroacetic acid.

REFERENCES

(1) Masters, C. L., Simms, G., Weinman, N. A., Multhaup, G., McDonald, B. L., and Beyreuther, K. (1985) Amyloid plaque core protein in Alzheimer disease and Down syndrome. *Proc. Natl. Acad. Sci. U.S.A. 82*, 4245−4249.

(2) Necula, M., Kayed, R., Milton, S., and Glabe, C. G. (2007) Small molecule inhibitors of aggregation indicate that amyloid β oligomerization and fibrillization pathways are independent and distinct. *J. Biol. Chem. 282*, 10311−10324.

(3) DeToma, A. S., Salamekh, S., Ramamoorthy, A., and Lim, M. H. (2012) Misfolded proteins in Alzheimer's disease and type II diabetes. *Chem. Soc. Rev. 41*, 608−621.

(4) Haass, C., and Selkoe, D. J. (2007) Soluble protein oligomers in neurodegeneration: Lessons from the Alzheimer's amyloid β-peptide. *Nat. Rev. Mol. Cell Biol. 8*, 101−112.

(5) Kodali, R., and Wetzel, R. (2007) Polymorphism in the intermediates and products of amyloid assembly. *Curr. Opin. Struct. Biol. 17*, 48−57.

(6) Lambert, M. P., Barlow, A. K., Chromy, B. A., Edwards, C., Freed, R., Liosatos, M., Morgan, T. E., Rozovsky, I., Trommer, B., Viola, K. L., Wals, P., Zhang, C., Finch, C. E., Krafft, G. A., and Klein, W. L. (1998) Diffusible, nonfibrillar ligands derived from Aβ(1−42) are potent central nervous system neurotoxins. *Proc. Natl. Acad. Sci. U.S.A. 95*, 6448−6453.

(7) Lotz, G. P., and Legleiter, J. (2013) The role of amyloidogenic protein oligomerization in neurodegenerative disease. *J. Mol. Med. 91*, 653−664.

(8) Kodali, R., Williams, A. D., Chemuru, S., and Wetzel, R. (2010) Aβ(1−40) Forms Five Distinct Amyloid Structures whose β-Sheet Contents and Fibril Stabilities Are Correlated. *J. Mol. Biol. 401*, 503−517.

(9) Meinhardt, J., Sachse, C., Hortschansky, P., Grigorieff, N., and Faendrich, M. (2009) A β(1−40) Fibril Polymorphism Implies Diverse Interaction Patterns in Amyloid Fibrils. *J. Mol. Biol. 386*, 869−877.

(10) Crowther, R. A., and Goedert, M. (2000) Abnormal Tau-Containing Filaments in Neurodegenerative Diseases. *J. Struct. Biol. 130*, 271−279.

(11) Lu, J.-X., Qiang, W., Yau, W.-M., Schwieters, C. D., Meredith, S. C., and Tycko, R. (2013) Molecular Structure of β-Amyloid Fibrils in Alzheimer's Disease Brain Tissue. *Cell 154*, 1257−1268.

(12) Petkova, A. T., Leapman, R. D., Guo, Z. H., Yau, W. M., Mattson, M. P., and Tycko, R. (2005) Self-propagating, molecular-level polymorphism in Alzheimer's β-amyloid fibrils. *Science 307*, 262−265.

(13) Burke, K. A., Yates, E. A., and Legleiter, J. (2013) Biophysical insights into how surfaces, including lipid membranes, modulate protein aggregation related to neurodegeneration. *Front. Neurol. 4*, 17.

(14) Legleiter, J., Fryer, J. D., Holtzman, D. M., and Kowalewski, T. (2011) The Modulating Effect of Mechanical Changes in Lipid Bilayers Caused by ApoE-Containing Lipoproteins on Aβ Induced Membrane Disruption. *ACS Chem. Neurosci. 2*, 588−599.

(15) Pifer, P. M., Yates, E. A., and Legleiter, J. (2011) Point Mutations in Aβ Result in the Formation of Distinct Polymorphic Aggregates in the Presence of Lipid Bilayers. *PLoS One 6*, e16248.

(16) Yates, E. A., Owens, S. L., Lynch, M. F., Cucco, E. M., Umbaugh, C. S., and Legleiter, J. (2013) Specific Domains of Aβ Facilitate Aggregation on and Association with Lipid Bilayers. *J. Mol. Biol. 425*, 1915−1933.

(17) Yip, C. M., Darabie, A. A., and McLaurin, J. (2002) Aβ 42-peptide assembly on lipid bilayers. *J. Mol. Biol. 318*, 97−107.

(18) Yip, C. M., and McLaurin, J. (2001) Amyloid-β peptide assembly: A critical step in fibrillogenesis and membrane disruption. *Biophys. J. 80*, 1359−1371.

(19) Yip, C. M., Elton, E. A., Darabie, A. A., Morrison, M. R., and McLaurin, J. (2001) Cholesterol, a modulator of membrane-associated Aβ-fibrillogenesis and neurotoxicity. *J. Mol. Biol. 311*, 723−734.

(20) Evangelisti, E., Cecchi, C., Cascella, R., Sgromo, C., Becatti, M., Dobson, C. M., Chiti, F., and Stefani, M. (2012) Membrane lipid composition and its physicochemical properties define cell vulnerability to aberrant protein oligomers. *J. Cell Sci. 125*, 2416−2427.

(21) Simakova, O., and Arispe, N. J. (2007) The cell-selective neurotoxicity of the Alzheimer's Aβ peptide is determined by surface phosphatidylserine and cytosolic ATP levels. Membrane binding is required for Aβ toxicity. *J. Neurosci. 27*, 13719−13729.

(22) Capone, R., Jang, H., Kotler, S. A., Kagan, B. L., Nussinov, R., and Lal, R. (2012) Probing Structural Features of Alzheimer's Amyloid-β Pores in Bilayers Using Site-Specific Amino Acid Substitutions. *Biochemistry 51*, 776−785.

(23) Connelly, L., Jang, H., Arce, F. T., Capone, R., Kotler, S. A., Ramachandran, S., Kagan, B. L., Nussinov, R., and Lal, R. (2012) Atomic Force Microscopy and MD Simulations Reveal Pore-Like Structures of All-D-Enantiomer of Alzheimer's β-Amyloid Peptide: Relevance to the Ion Channel Mechanism of AD Pathology. *J. Phys. Chem. B 116*, 1728−1735.

(24) Jang, H., Zheng, J., and Nussinov, R. (2007) Models of β-amyloid ion channels in the membrane suggest that channel formation in the bilayer is a dynamic process. *Biophys. J. 93*, 1938−1949.

(25) Kotler, S. A., Walsh, P., Brender, J. R., and Ramamoorthy, A. (2014) Differences between amyloid-β aggregation in solution and on the membrane: Insights into elucidation of the mechanistic details of Alzheimer's disease. *Chem. Soc. Rev. 43*, 6692−6700.

(26) Martins, I. C., Kuperstein, I., Wilkinson, H., Maes, E., Vanbrabant, M., Jonckheere, W., Van Gelder, P., Hartmann, D., D'Hooge, R., De Strooper, B., Schymkowitz, J., and Rousseau, F. (2008) Lipids revert inert Aβ amyloid fibrils to neurotoxic protofibrils that affect learning in mice. *EMBO J. 27*, 224−233.

(27) Bokvist, M., Lindstrom, F., Watts, A., and Grobner, G. (2004) Two types of Alzheimer's β-amyloid (1−40) peptide membrane interactions: Aggregation preventing transmembrane anchoring versus accelerated surface fibril formation. *J. Mol. Biol. 335*, 1039−1049.

(28) Burke, K. A., Yates, E. A., and Legleiter, J. (2013) Amyloid-Forming Proteins Alter the Local Mechanical Properties of Lipid Membranes. *Biochemistry 52*, 808−817.

(29) Lindstrom, F., Bokvist, M., Sparrman, T., and Grobner, G. (2002) Association of amyloid-β peptide with membrane surfaces

monitored by solid state NMR. *Phys. Chem. Chem. Phys. 4*, 5524−5530.
(30) Accardo, A., Shalabaeva, V., Cotte, M., Burghammer, M., Krahne, R., Riekel, C., and Dante, S. (2014) Amyloid-β Peptide Conformational Changes in the Presence of a Lipid Membrane System. *Langmuir 30*, 3191−3198.
(31) Canale, C., Seghezza, S., Vilasi, S., Carrotta, R., Bulone, D., Diaspro, A., Biagio, P. L. S., and Dante, S. (2013) Different effects of Alzheimer's peptide Aβ(1−40) oligomers and fibrils on supported lipid membranes. *Biophys. Chem. 182*, 23−29.
(32) Dante, S., Hauss, T., Steitz, R., Canale, C., and Dencher, N. A. (2011) Nanoscale structural and mechanical effects of β-amyloid (1−42) on polymer cushioned membranes: A combined study by neutron reflectometry and AFM Force Spectroscopy. *Biochim. Biophys. Acta 1808*, 2646−2655.
(33) Moores, B., Drolle, E., Attwood, S. J., Simons, J., and Leonenko, Z. (2011) Effect of Surfaces on Amyloid Fibril Formation. *PLoS One 6*, e25954.
(34) Drolle, E., Gaikwad, R. M., and Leonenko, Z. (2012) Nanoscale Electrostatic Domains in Cholesterol-Laden Lipid Membranes Create a Target for Amyloid Binding. *Biophys. J. 103*, L27−L29.
(35) Hane, F., Drolle, E., Gaikwad, R., Faught, E., and Leonenko, Z. (2011) Amyloid-β Aggregation on Model Lipid Membranes: An Atomic Force Microscopy Study. *J. Alzheimer's Dis. 26*, 485−494.
(36) Stine, W. B., Dahlgren, K. N., Krafft, G. A., and LaDu, M. J. (2003) In vitro characterization of conditions for amyloid-β peptide oligomerization and fibrillogenesis. *J. Biol. Chem. 278*, 11612−11622.
(37) Legleiter, J., Park, M., Cusick, B., and Kowalewski, T. (2006) Scanning probe acceleration microscopy (SPAM) in fluids: Mapping mechanical properties of surfaces at the nanoscale. *Proc. Natl. Acad. Sci. U.S.A. 103*, 4813−4818.
(38) Hutter, J. L., and Bechhoefer, J. (1993) Calibration of atomic-force microscope tips. *Rev. Sci. Instrum. 64*, 1868−1873.
(39) Burke, K. A., Godbey, J., and Legleiter, J. (2011) Assessing mutant huntingtin fragment and polyglutamine aggregation by atomic force microscopy. *Methods 53*, 275−284.
(40) Legleiter, J., DeMattos, R. B., Holtzman, D. M., and Kowalewski, T. (2004) In situ AFM studies of astrocyte-secreted apolipoprotein E- and J-containing lipoproteins. *J. Colloid Interface Sci. 278*, 96−106.
(41) Yu, L., Edalji, R., Harlan, J. E., Holzman, T. F., Lopez, A. P., Labkovsky, B., Hillen, H., Barghorn, S., Ebert, U., Richardson, P. L., Miesbauer, L., Solomon, L., Bartley, D., Walter, K., Johnson, R. W., Hajduk, P. J., and Olejniczak, E. T. (2009) Structural Characterization of a Soluble Amyloid β-Peptide Oligomer. *Biochemistry 48*, 1870−1877.
(42) Cheng, I. H., Scearce-Levie, K., Legleiter, J., Palop, J. J., Gerstein, H., Bien-Ly, N., Puolivali, J., Lesne, S., Ashe, K. H., Muchowski, P. J., and Mucke, L. (2007) Accelerating amyloid-β fibrillization reduces oligomer levels and functional deficits in Alzheimer disease mouse models. *J. Biol. Chem. 282*, 23818−23828.
(43) Groves, J. T., Ulman, N., and Boxer, S. G. (1997) Micropatterning fluid lipid bilayers on solid supports. *Science 275*, 651−653.
(44) Jass, J., Tjarnhage, T., and Puu, G. (2000) From liposomes to supported, planar bilayer structures on hydrophilic and hydrophobic surfaces: An atomic force microscopy study. *Biophys. J. 79*, 3153−3163.
(45) Panchal, M., Loeper, J., Cossec, J.-C., Perruchini, C., Lazar, A., Pompon, D., and Duyckaerts, C. (2010) Enrichment of cholesterol in microdissected Alzheimer's disease senile plaques as assessed by mass spectrometry. *J. Lipid Res. 51*, 598−605.
(46) Gellermann, G. P., Appel, T. R., Tannert, A., Radestock, A., Hortschansky, P., Schroeckh, V., Leisner, C., Lütkepohl, T., Shtrasburg, S., Röcken, C., Pras, M., Linke, R. P., Diekmann, S., and Fändrich, M. (2005) Raft lipids as common components of human extracellular amyloid fibrils. *Proc. Natl. Acad. Sci. U.S.A. 102*, 6297−6302.
(47) Chaibva, M., Burke, K. A., and Legleiter, J. (2014) Curvature Enhances Binding and Aggregation of Huntingtin at Lipid Membranes. *Biochemistry 53*, 2355−2365.
(48) Shamitko-Klingensmith, N., Molchanoff, K. M., Burke, K. A., Magnone, G. J., and Legleiter, J. (2012) Mapping the Mechanical Properties of Cholesterol-Containing Supported Lipid Bilayers with Nanoscale Spatial Resolution. *Langmuir 28*, 13411−13422.
(49) Guzman, H. V., Perrino, A. P., and Garcia, R. (2013) Peak Forces in High-Resolution Imaging of Soft Matter in Liquid. *ACS Nano 7*, 3198−3204.
(50) Colletier, J.-P., Laganowsky, A., Landau, M., Zhao, M., Soriaga, A. B., Goldschmidt, L., Flot, D., Cascio, D., Sawaya, M. R., and Eisenberg, D. (2011) Molecular basis for amyloid-β polymorphism. *Proc. Natl. Acad. Sci. U.S.A. 108*, 16938−16943.
(51) Goldsbury, C., Frey, P., Olivieri, V., Aebi, U., and Muller, S. A. (2005) Multiple assembly pathways underlie amyloid-β fibril polymorphisms. *J. Mol. Biol. 352*, 282−298.
(52) Meinhardt, J., Tartaglia, G. G., Pawar, A., Christopeit, T., Hortschansky, P., Schroeckh, V., Dobson, C. M., Vendruscolo, M., and Faendrich, M. (2007) Similarities in the thermodynamics and kinetics of aggregation of disease-related Aβ(1−40) peptides. *Protein Sci. 16*, 1214−1222.
(53) Volpatti, L. R., Vendruscolo, M., Dobson, C. M., and Knowles, T. P. J. (2013) A Clear View of Polymorphism, Twist, and Chirality in Amyloid Fibril Formation. *ACS Nano 7*, 10443−10448.
(54) Qiang, W., Kelley, K., and Tycko, R. (2013) Polymorph-Specific Kinetics and Thermodynamics of β-Amyloid Fibril Growth. *J. Am. Chem. Soc. 135*, 6860−6871.
(55) Ahmed, M., Davis, J., Aucoin, D., Sato, T., Ahuja, S., Aimoto, S., Elliott, J. I., Van Nostrand, W. E., and Smith, S. O. (2010) Structural conversion of neurotoxic amyloid-β(1−42) oligomers to fibrils. *Nat. Struct. Mol. Biol. 17*, 561−567.
(56) Bitan, G., Kirkitadze, M. D., Lomakin, A., Vollers, S. S., Benedek, G. B., and Teplow, D. B. (2003) Amyloid β-protein (Aβ) assembly: Aβ 40 and Aβ 42 oligomerize through distinct pathways. *Proc. Natl. Acad. Sci. U.S.A. 100*, 330−335.
(57) Berhanu, W. M., and Hansmann, U. H. E. (2012) Structure and Dynamics of Amyloid-β Segmental Polymorphisms. *PLoS One 7*, e41479.
(58) Krafft, G. A., and Klein, W. L. (2010) ADDLs and the signaling web that leads to Alzheimer's disease. *Neuropharmacology 59*, 230−242.
(59) Lesne, S., Koh, M. T., Kotilinek, L., Kayed, R., Glabe, C. G., Yang, A., Gallagher, M., and Ashe, K. H. (2006) A specific amyloid-β protein assembly in the brain impairs memory. *Nature 440*, 352−357.
(60) Noguchi, A., Matsumura, S., Dezawa, M., Tada, M., Yanazawa, M., Ito, A., Akioka, M., Kikuchi, S., Sato, M., Ideno, S., Noda, M., Fukunari, A., Muramatsu, S.-i., Itokazu, Y., Sato, K., Takahashi, H., Teplow, D. B., Nabeshima, Y.-i., Kakita, A., Imahori, K., and Hoshi, M. (2009) Isolation and Characterization of Patient-derived, Toxic, High Mass Amyloid β-Protein (Aβ) Assembly from Alzheimer Disease Brains. *J. Biol. Chem. 284*, 32895−32905.
(61) Selkoe, D. J. (2008) Soluble oligomers of the amyloid β-protein impair synaptic plasticity and behavior. *Behav. Brain Res. 192*, 106−113.
(62) Chimon, S., Shaibat, M. A., Jones, C. R., Calero, D. C., Aizezi, B., and Ishii, Y. (2007) Evidence of fibril-like β-sheet structures in a neurotoxic amyloid intermediate of Alzheimer's β-amyloid. *Nat. Struct. Mol. Biol. 14*, 1157−1164.
(63) Qiang, W., Yau, W.-M., Luo, Y., Mattson, M. P., and Tycko, R. (2012) Antiparallel β-sheet architecture in Iowa-mutant β-amyloid fibrils. *Proc. Natl. Acad. Sci. U.S.A. 109*, 4443−4448.
(64) Walsh, D. M., Hartley, D. M., Kusumoto, Y., Fezoui, Y., Condron, M. M., Lomakin, A., Benedek, G. B., Selkoe, D. J., and Teplow, D. B. (1999) Amyloid β-protein fibrillogenesis: Structure and biological activity of protofibrillar intermediates. *J. Biol. Chem. 274*, 25945−25952.
(65) Bieschke, J., Russ, J., Friedrich, R. P., Ehrnhoefer, D. E., Wobst, H., Neugebauer, K., and Wanker, E. E. (2010) EGCG remodels mature α-synuclein and amyloid-β fibrils and reduces cellular toxicity. *Proc. Natl. Acad. Sci. U.S.A. 107*, 7710−7715.

(66) Ehrnhoefer, D. E., Duennwald, M., Markovic, P., Wacker, J. L., Engemann, S., Roark, M., Legleiter, J., Marsh, J. L., Thompson, L. M., Lindquist, S., Muchowski, P. J., and Wanker, E. E. (2006) Green tea (−)-epigallocatechin-gallate modulates early events in huntingtin misfolding and reduces toxicity in Huntington's disease models. *Hum. Mol. Genet. 15*, 2743−2751.
(67) Engel, M. F. M., VandenAkker, C. C., Schleeger, M., Velikov, K. P., Koenderink, G. H., and Bonn, M. (2012) The Polyphenol EGCG Inhibits Amyloid Formation Less Efficiently at Phospholipid Interfaces than in Bulk Solution. *J. Am. Chem. Soc. 134*, 14781−14788.
(68) Sciacca, M. F. M., Kotler, S. A., Brender, J. R., Chen, J., Lee, D.-k., and Ramamoorthy, A. (2012) Two-Step Mechanism of Membrane Disruption by Aβ through Membrane Fragmentation and Pore Formation. *Biophys. J. 103*, 702−710.
(69) Sasahara, K., Morigaki, K., and Shinya, K. (2013) Effects of membrane interaction and aggregation of amyloid β-peptide on lipid mobility and membrane domain structure. *Phys. Chem. Chem. Phys. 15*, 8929−8939.
(70) Morriss-Andrews, A., Brown, F. L. H., and Shea, J.-E. (2014) A Coarse-Grained Model for Peptide Aggregation on a Membrane Surface. *J. Phys. Chem. B 118*, 8420−8432.
(71) Jan, A., Adolfsson, O., Allaman, I., Buccarello, A.-L., Magistretti, P. J., Pfeifer, A., Muhs, A., and Lashuel, H. A. (2011) Aβ42 Neurotoxicity Is Mediated by Ongoing Nucleated Polymerization Process Rather than by Discrete Aβ42 Species. *J. Biol. Chem. 286*, 8585−8596.
(72) Jarrett, J. T., Berger, E. P., and Lansbury, P. T. (1993) The carboxy terminus of the β-amyloid protein is critical for the seeding of amyloid formation: Implications for the pathogenesis of Alzheimers disease. *Biochemistry 32*, 4693−4697.
(73) Paravastu, A. K., Qahwash, I., Leapman, R. D., Meredith, S. C., and Tycko, R. (2009) Seeded growth of β-amyloid fibrils from Alzheimer's brain-derived fibrils produces a distinct fibril structure. *Proc. Natl. Acad. Sci. U.S.A. 106*, 7443−7448.
(74) Jucker, M., and Walker, L. C. (2011) Pathogenic protein seeding in Alzheimer disease and other neurodegenerative disorders. *Ann. Neurol. 70*, 532−540.
(75) Serem, W. K., Bett, C. K., Ngunjiri, J. N., and Garno, J. C. (2011) Studies of the growth, evolution, and self-aggregation of β-amyloid fibrils using tapping-mode atomic force microscopy. *Microsc. Res. Tech. 74*, 699−708.
(76) Stoehr, J., Watts, J. C., Mensinger, Z. L., Oehler, A., Grillo, S. K., DeArmond, S. J., Prusiner, S. B., and Giles, K. (2012) Purified and synthetic Alzheimer's amyloid β (Aβ) prions. *Proc. Natl. Acad. Sci. U.S.A. 109*, 11025−11030.
(77) Cobb, N. J., Apostol, M. I., Chen, S., Smirnovas, V., and Surewicz, W. K. (2014) Conformational stability of mammalian prion protein amyloid fibrils is dictated by a packing polymorphism within the core region. *J. Biol. Chem. 289*, 2643−2650.
(78) Braak, H., and Del Tredici, K. (2011) Alzheimer's pathogenesis: Is there neuron-to-neuron propagation? *Acta Neuropathol. 121*, 589−595.
(79) Kane, M. D., Lipinski, W. J., Callahan, M. J., Bian, F., Durham, R. A., Schwarz, R. D., Roher, A. E., and Walker, L. C. (2000) Evidence for Seeding of β-Amyloid by Intracerebral Infusion of Alzheimer Brain Extracts in β-Amyloid Precursor Protein-Transgenic Mice. *J. Neurosci. 20*, 3606−3611.
(80) Langer, F., Eisele, Y. S., Fritschi, S. K., Staufenbiel, M., Walker, L. C., and Jucker, M. (2011) Soluble Aβ Seeds Are Potent Inducers of Cerebral β-Amyloid Deposition. *J. Neurosci. 31*, 14488−14495.